# Hybrid organic spin valves

Popinciuc, Mihaita

# 2

# Theoretical aspects

In the first part of this chapter theoretical aspects of electrical spin injection and detection are presented in the frame of a resistor model. In this model, the elements of the spin valve, i.e., the ferromagnetic injector/detector and the semiconductor, are treated as simple resistors. Even though specific information related to the metal/semiconductor interface and to the transport mechanism in the semiconductor are not taken into account, we believe that this resistor model provides a good starting point in realizing organic spin valves. It will be shown that successful realization of semiconductor spin valves necessitates overcoming the conductivity mismatch problem: the spin dependent resistance of the injector/detector should be matched to a certain extent with the spin independent resistance of the semiconducting layer. In the second part of this chapter, the photoelectron spectroscopy is introduced as a tool for investigating the interfacial properties (carrier injection barriers, chemistry, band bending) at hybrid metal-organic or metal-oxide-organic interfaces. The information gained from photoelectron spectroscopy experiments can help in the design of hybrid organic spin valve devices.

## 2.1 Theory of spin valve devices

The functioning of all electrical spin valves relies on creating a spin accumulation by passing current from a ferromagnetic electrode (the spin source) into a non magnetic material (the transport and manipulation medium of the spin accumulation) subsequently followed by detection using a second ferromagnetic electrode. In the first part of this chapter we will underline the principles of electrical injection/detection of spin accumulation in the frame of a two channel current model. Our discussion follows the theoretical concepts of van Son *et al.* [1]. Next, we will introduce a resistor model of a spin valve device, in which the spin flip in the semiconductor is neglected. Within this simple model Schmidt *et al.* [2] have shown that injection/detection of spin polarized current from ferromagnetic metals into semiconductors is prohibited by the conductivity mismatch problem. The model is phenomenologically developed further in order to include the effect of the spin relaxation in semiconductor. We will show, in qualitative agreement obtained with the more rigorous approach developed by Fert and Jaffrès [4], that tuning of the resistances of the spin valve circuit is necessary in order to obtain a measurable spin signal.

### 2.1.1 Basic concepts of spintronics

#### Basics of spin transport

In a diffusive conductor in the linear regime the transport is governed by the electrons at the Fermi level [6]. In the approximation that most scattering events preserve the spin orientation (that is momentum relaxation time is much smaller than the spin flip time) the current can be considered as being carried in parallel by two independent spin channels: one for spin up electrons ($\uparrow$) and one for spin down electrons ($\downarrow$), a formalism applied to describe the transport properties of ferromagnets [7]. The current flow is determined by the gradient of the electrochemical potential, therefore in one dimension, we can write Ohm's law in local form for each channel as

$$j_{\uparrow,\downarrow} = \frac{\sigma_{\uparrow,\downarrow}}{e} \frac{\partial \mu_{\uparrow,\downarrow}}{\partial x}, \tag{2.1}$$

where $j_{\uparrow,\downarrow}$, $\sigma_{\uparrow,\downarrow}$ and $\mu_{\uparrow,\downarrow}$ represent the current density, the conductivity and the chemical potential of the spin $\uparrow,\downarrow$ channel. Besides the total charge current given by

$$j = j_{\uparrow} + j_{\downarrow}, \tag{2.2}$$

a spin current can be defined as

$$j_s = j_{\uparrow} - j_{\downarrow}. \tag{2.3}$$

In ferromagnets, as a direct consequence of the exchange energy splitting [8], the condition $\sigma_\uparrow \neq \sigma_\downarrow$ is generally met. Therefore, when a current is passed through a ferromagnet, beside the charge current a different from zero spin current also flows. The current is spin polarized and the degree of polarization ($\beta$) is given by

$$\beta = \frac{I_\uparrow - I_\downarrow}{I_\uparrow + I_\downarrow} = \frac{j_\uparrow - j_\downarrow}{j_\uparrow + j_\downarrow} = \frac{\sigma_\uparrow - \sigma_\downarrow}{\sigma_\uparrow + \sigma_\downarrow} = \frac{\sigma_\uparrow - \sigma_\downarrow}{\sigma} \tag{2.4}$$

where $\sigma = \sigma_\uparrow + \sigma_\downarrow$ is the total conductivity. Introducing $\beta$, we can write Eq. 2.1 as

$$j_\uparrow = (1+\beta)\frac{\sigma}{2}\,\frac{1}{e}\,\frac{\partial \mu_\uparrow}{\partial x} \tag{2.5a}$$

$$j_\downarrow = (1-\beta)\frac{\sigma}{2}\,\frac{1}{e}\,\frac{\partial \mu_\downarrow}{\partial x} \tag{2.5b}$$

which shows that in ferromagnets the total current is distributed unequally over the two spin channels. In other words, in ferromagnets, the charge current carries also a magnetization ($j_s \neq 0$), a characteristic which makes them good candidates for spin sources.

In a non-magnetic material $\sigma_{N\uparrow} = \sigma_{N\downarrow}$. Therefore, the spin polarization of the current is zero ($\beta = 0$), that is the current is carried equally by the two spin channels. In order to induce spin current in a non-magnet, the condition $\partial\mu_\uparrow/\partial x \neq \partial\mu_\downarrow/\partial x$ must be fulfilled, which is the same as connecting different bias voltages over two channels. This is realized by driving a current from a ferromagnet into the non-magnet, situation which can be readily understood when considering a resistor model of the interface (presented later).

**Spin injection, spin accumulation, spin detection**

When a current is passed from a ferromagnet (F) into a non-magnet (N), far from the interface, the current is spin polarized in F and unpolarized in N. Assuming conservation of the spin up and spin down currents across the interface (transparent interface), it follows that in a region near the interface current conversion takes place by spin flip processes. Due to the equal conductivities of the two spin channels in N, spins pile up in F and accumulate in N on the two sides of the interface. The spin accumulation decays exponentially with the distance form the interface obeying the diffusion equation [1, 4, 12, 13]

$$\frac{\partial^2 \Delta\mu}{\partial x^2} = \frac{\Delta\mu}{\lambda_{sf}^2}, \tag{2.6}$$

where $\lambda_{sf} = \sqrt{D\tau_{sf}}$ is the spin relaxation length (spin flip length), with $D$ the diffusion constant and $\tau_{sf}$ the spin relaxation time.

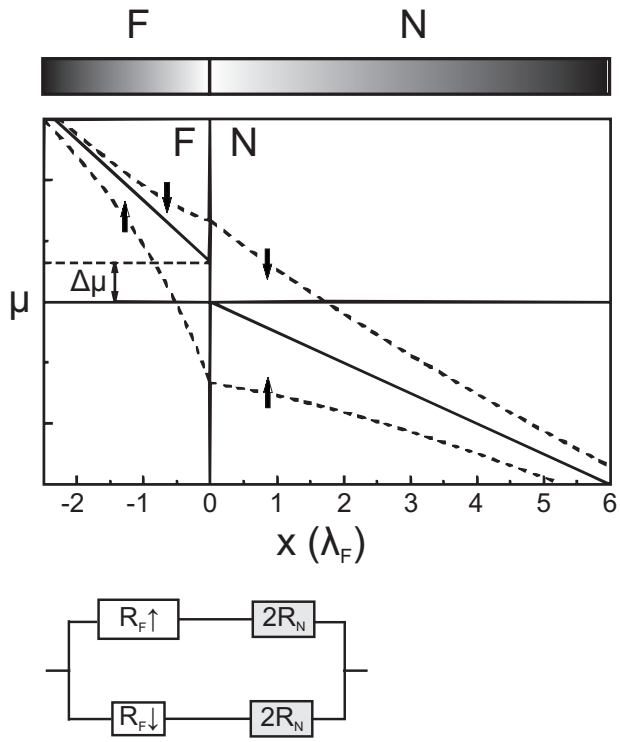


Figure 2.1: (a) Driving a current from a ferromagnet into a non-magnet leads to spin accumulation (induced magnetization) in both materials over the characteristic spin flip length $\lambda_F, \lambda_N$. The plot corresponds to $\lambda_N = 5\lambda_F$ (adapted from [13]). (b) Resistor model of the interface.

A spin accumulation exists in both F and N and decays exponentially with the characteristics lengths: $\lambda_{sf}^F$ and $\lambda_{sf}^N$, simply denoted as $\lambda_F$ and $\lambda_N$ from now on. The process is described in Fig. 2.1. As a consequence of the spin accumulation a spin related interfacial resistance arises

$$\Delta R_{int} = \frac{\beta^2(\sigma_N^{-1}\lambda_N)(\sigma_F^{-1}\lambda_F)}{(\sigma_F^{-1}\lambda_F) + (1-\beta^2)(\sigma_N^{-1}\lambda_N)}. \tag{2.7}$$

This interfacial resistance causes a voltage drop at the interface, when a bias is applied, a voltage drop which is only related to the induced spin accumulation. Experimentally, the detection of the spin accumulation can be realized in a spin valve measurement, in which two ferromagnets are in contact with the normal material and placed at a distance much smaller than $\lambda_N$. By switching the magnetization of the ferromagnets from parallel (P) to antiparallel (AP), the

difference between the two measured resistances is

$$\Delta R = R_{AP} - R_P = 2\Delta R_{int}, \tag{2.8}$$

a relation which allows for the extraction of $\lambda_N$, the parameter of interest.

**Resistor model of a F/N interface**

The same results can be achieved by considering an equivalent resistor model of the F/N system. By writing the resistances for the two spin channels as

$$R_{F\uparrow} = 2R_F/(1+\beta) \tag{2.9a}$$

$$R_{F\downarrow} = 2R_F/(1-\beta) \tag{2.9b}$$

$$R_{N\uparrow} = R_{N\downarrow} = 2R_N \tag{2.9c}$$

where we have been taking into account the spin dependent (independent) resistances in F (N) for the two channels and by taking

$$a = \frac{R_F}{R_N}, \tag{2.10}$$

a simple calculation of the resistor model of Fig. 2.1 leads to

$$R_{int} = R_{eq} - (R_F + R_N) \quad = \beta^2 R_N \frac{a}{a+1-\beta^2} \tag{2.11a}$$

$$= \beta^2 R_F \frac{1}{a+1-\beta^2} \tag{2.11b}$$

where $R_{eq}$ is the equivalent resistance of the circuit shown in Fig. 2.1. The above equation is identical to Eq. 2.7 when taking

$$R_F = \sigma_F^{-1}\lambda_F \quad \text{and} \quad R_N = \sigma_N^{-1}\lambda_N, \tag{2.12}$$

where $R_F, R_N$ are the resistances per unit area over a spin flip length of the ferromagnet and non-magnet, respectively. The different spin dependent resistances for the spin up and spin down channels in the ferromagnet cause different voltage drop over the two channels in N, see the resistor model of Fig. 2.1, therefore creating a spin accumulation in N. The spin related signal (Eq. 2.11b) depends on the ratio $a = R_F/R_N$ and is higher when N is a semiconductor instead of a metal, assuming the same injection current. This is one of the reasons why spin injection in semiconductors is appealing, it promises larger signals. However, the larger signals in semiconductors are superimposed on larger background signals, and the magnetoresistance ratio is the relevant parameter in a two terminal measurement.

### 2.1.2 Spin valves. Conductivity mismatch

To induce a spin accumulation in N, a single F/N contact is sufficient. However, in order to take advantage of the spin accumulation properties, detection of the spin accumulation is necessary. This is realized in a F/N/F structure, also known as spin valve device, in which the pair of ferromagnetic electrodes are placed at a distance $L$, with $L < \lambda_N$. A two terminal measurement configuration is shown in Fig. 2.2. The sample is connected to an external measurement circuit and the resistance of the device is monitored with respect to the relative orientation of the magnetization of the ferromagnetic electrodes, parallel (P) or antiparallel (AP). In the following we analyze the spin valve device using a simple resistor model in which relaxation effects are neglected [2]. Later, we generalize this model by including the spin relaxation.

**Resistor model of a spin valve device without spin relaxation**

Using the notations previously made (Eq. 2.9), the equivalent resistances of the two channels are as depicted in Fig. 2.2. Assuming semi-infinite ferromagnetic electrodes and a non-magnet of length L, the $R_F$ and $R_N$ resistances are given by

$$R_F = \sigma_F^{-1}\lambda_F \quad \text{and} \quad R_N = \sigma_N^{-1}L. \tag{2.13}$$

In the parallel orientation the resistance of the spin down channel is smaller than the resistance of the spin up channel and smaller than the resistance of the spin up (equal to the one of the spin down) channels in the AP orientation. This determines that the total resistance $R_P < R_{AP}$, i.e., the spin down channel practically short circuits the spin up channel. Solving the resistor model of Fig. 2.2 for both orientations (P and AP) the difference $\Delta R = R_{AP} - R_P$ (the spin valve signal) becomes

$$\Delta R = R_{AP} - R_P = \frac{\beta^2}{1-\beta^2} R_N \frac{4a^2}{2a+1-\beta^2} \tag{2.14a}$$

$$= \frac{\beta^2}{1-\beta^2} R_F \frac{4a}{2a+1-\beta^2} \tag{2.14b}$$

and the magnetoresistance ratio ($\Delta R/R_P$) reads

$$\frac{\Delta R}{R_P} = \frac{R_{AP} - R_P}{R_P} = \frac{\beta^2}{1-\beta^2} \frac{(2a)^2}{(2a+1)^2 - \beta^2} \tag{2.15}$$

In the case of using ferromagnetic metals and semiconductors to build spin valves the condition

$$R_N \gg R_F \;\; (a \to 0) \tag{2.16}$$

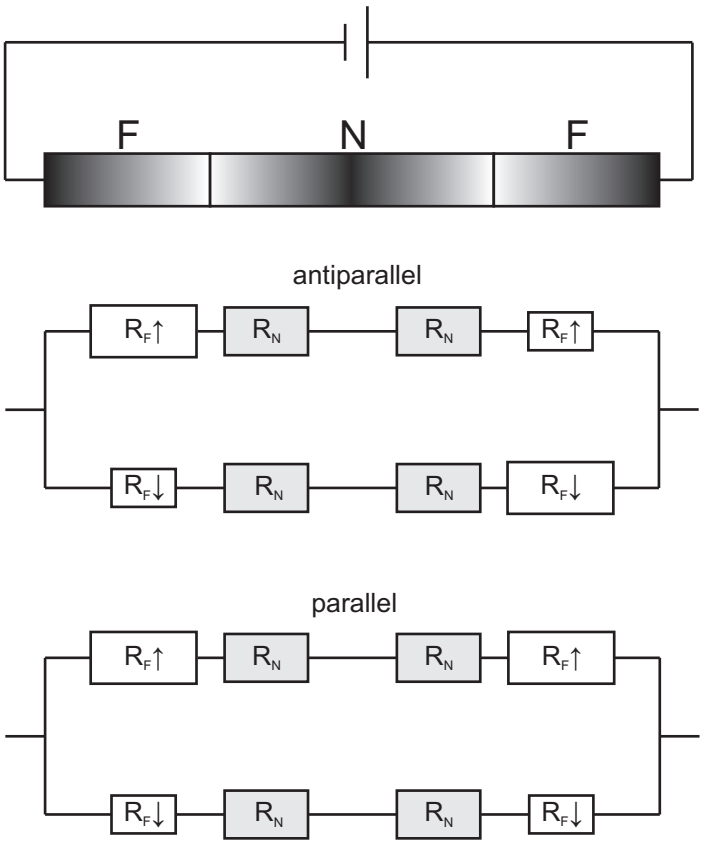


Figure 2.2: The spin valve device: the electrical circuit and the equivalent resistor models for parallel and antiparallel orientation of the magnetization of the ferromagnets.

is always met, fact which leads to a vanishing magnetoresistance

$$\frac{\Delta R}{R_P} \to 0. \tag{2.17}$$

This is known as the conductivity mismatch problem: it is not possible to efficiently inject (detect) spins in semiconductors by using ferromagnetic metals as injector (detector) since the condition 2.16 is naturally fulfilled. The solution to this problem is to increase the spin dependent resistance (injector/detector) of the circuit. It has been suggested that inserting a tunnel barrier in between the metal [2, 4, 5] and semiconductor would solve this problem since the tunneling of the carriers is spin dependent. Alternative approaches include the use of mag-

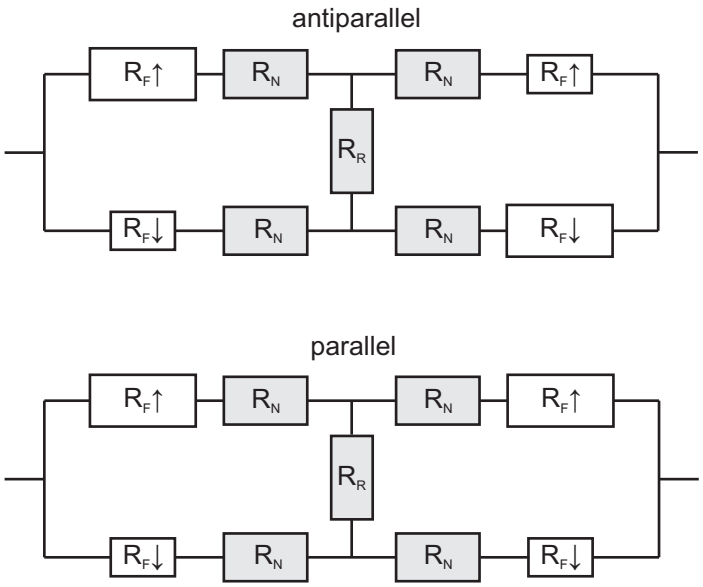


Figure 2.3: Resistor model with spin relaxation in semiconductor included.

netic semiconductors, half metallic ferromagnets [2, 3]. According to Eq. 2.15, when $a \to \infty$ ($R_N \ll R_F$) the maximum magnetoresistance signal is obtained

$$\frac{\Delta R}{R_P} \to \frac{\beta^2}{1-\beta^2}. \tag{2.18}$$

**Resistor model of a spin valve device with spin relaxation**

A more rigorous approach [4] showed that in the limit $a \to \infty$ ($R_N \ll R_F$) the magnetoresistance also vanishes. The simple model presented above becomes a more realistic one if spin relaxation in the semiconductor is taken into account. In the resistor model network the spin relaxation is introduced by connecting an equivalent (relaxation) resistor ($R_R$) according to Fig. 2.3.

By solving the resistor network for the P and AP orientations of the magnetization of the ferromagnetic electrodes and by defining

$$b = \frac{R_R}{R_N} \tag{2.19}$$

one obtains

$$\Delta R = \frac{\beta^2 b}{2a + (b+1)(1-\beta^2)} R_N \frac{(2a)^2}{2a + 1 - \beta^2} \tag{2.20}$$

$$\frac{\Delta R}{R_P} = \frac{\beta^2 b}{2a + (b+1)(1-\beta^2)} \frac{(2a)^2}{(2a+1)^2 - \beta^2}. \tag{2.21}$$

It is easy to see that in the limit $R_R \to \infty$ (corresponding to no relaxation which was assumed in the previous model) Eqs. 2.20-2.21 reduce to Eqs. 2.14-2.15. Now let us discuss a few limiting cases

1. $a \to \infty$, $b$ finite. In this case $R_F \gg R_N$, which may correspond to high resistive tunnel barriers and metals, the magnetoresistance ratio vanishes.

2. $a \to 0$, $b$ finite. This corresponds to $R_F \ll R_N$, for example when using ferromagnetic metals and semiconductors, the magnetoresistance ratio vanishes.

3. $b \to \infty$, $a$ finite. This corresponds to no relaxation in semiconductor ($R_R \to \infty$) and a maximum magnetoresistance ratio is obtained when $a \gg 1$

$$\frac{\Delta R}{R_P} = \frac{\beta^2}{1-\beta^2}. \tag{2.22}$$

4. $b \to 0$, $a$ finite. In this case $R_R \ll R_N$ which means very fast relaxation in semiconductor (practically $R_R$ shorts the circuit). The magnetoresistance ratio becomes zero again.

5. $a$ and $b$ both finite. This is the situation of most interest. Given a semiconductor in which the spin injection is desired, the parameter $b = R_R/R_N$ is a given quantity. It is now of interest to determine $a = R_F/R_N$ for which the magnetoresistance signal is maximum. This situation is dealt with in the next paragraphs.

Assuming that the semiconductor has a length $L \ll \lambda_N$ and that the electrochemical potentials for spin up and spin down channels induced by the ferromagnet at the interface, for simplicity taken as $\pm\mu_0$, decrease exponentially with the distance

$$\mu_{\uparrow,\downarrow}(x) = \pm\mu_0 \, e^{-x/\lambda_N}, \tag{2.23}$$

the semiconductor can be modeled as in Fig. 2.4. By solving Ohm's and Kirchoff's laws for the three currents indicated in Fig. 2.4, we obtain the following expression for the spin relaxation resistance

$$R_R \approx 8 R_N \lambda_N^2 / L^2. \tag{2.24}$$

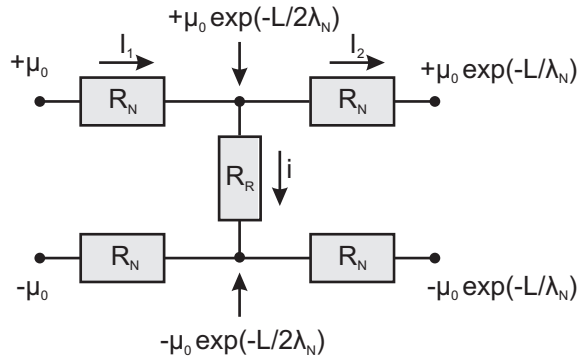


Figure 2.4: Resistor model of the semiconductor side of a single F/N interface with spin relaxation in the semiconductor included. See text for details.

In the limit $\lambda_N \to \infty$ or $L = 0$ (meaning no relaxation in the semiconductor or sitting just at the interface), $R_R \to \infty$ as expected. By combining Eq. 2.24 with Eq. 2.20 the following relations are obtained for $\Delta R$ and the magnetoresistance ratio

$$\Delta R = \frac{8\beta^2\lambda_N^2/L^2}{(2a+1-\beta^2)+8(1-\beta^2)\lambda_N^2/L^2}\, R_N\, \frac{(2a)^2}{2a+1-\beta^2} \tag{2.25}$$

$$\frac{\Delta R}{R_P} = \frac{8\beta^2\lambda_N^2/L^2}{(2a+1-\beta^2)+8(1-\beta^2)\lambda_N^2/L^2}\, \frac{(2a)^2}{(2a+1)^2-\beta^2} \tag{2.26}$$

The parameter $a$ depends on the resistivity of the ferromagnet and non-magnet as $a = R_F/R_N = (\rho_F\lambda_F)/(\rho_N L)$. Taking $\beta = 0.46$, $\lambda_F = 60$ nm [4] (values which correspond to Co) and $\lambda_N = 2.5$ $\mu$m, a plot of $\Delta R/R_P$ as a function of $\rho_F/\rho_N$ (for different thicknesses $L$ of the semiconductor) yields Fig. 2.5a). In agreement with just inspecting the resistor network of Fig. 2.3, the figure shows that negligible spin signal is expected when $\rho_F \ll \rho_N$ (virtually replacing $R_F$ by a short) or when $\rho_F \gg \rho_N$ (virtually replacing $R_N$ and therefore $R_R$ by shorts). Clearly, tuning of $\rho_F$ or $\rho_N$ is necessary in order to maximize the magnetoresistance signal for given values of $\beta$, $\lambda_F$ and $L$. The signal is maximum when $\rho_F/\rho_N$ is on the order of 100 (that is $a$ is the order of unity taking into account the values of $\lambda_F$ and $L$). With decreasing $L$ the maximum signal becomes limited by the value of $\beta$ according to Eq. 2.22.

Assuming $\lambda_N = 2.5$ $\mu$m, $L = 250$ nm, a plot of $\Delta R/R_P$ as a function of $\beta$ for various values of $\rho_F/\rho_N$ yields Fig. 2.5b). The small spin signal determined by an unfavorable value of $\rho_F/\rho_N$ can be compensated by an increased value of $\beta$ to a certain extent. For $\rho_F/\rho_N = 0.001$, $\beta$ should be in excess of 97 % for a spin signal of 0.01 %. The conductivity mismatch problem becomes progressively worse with

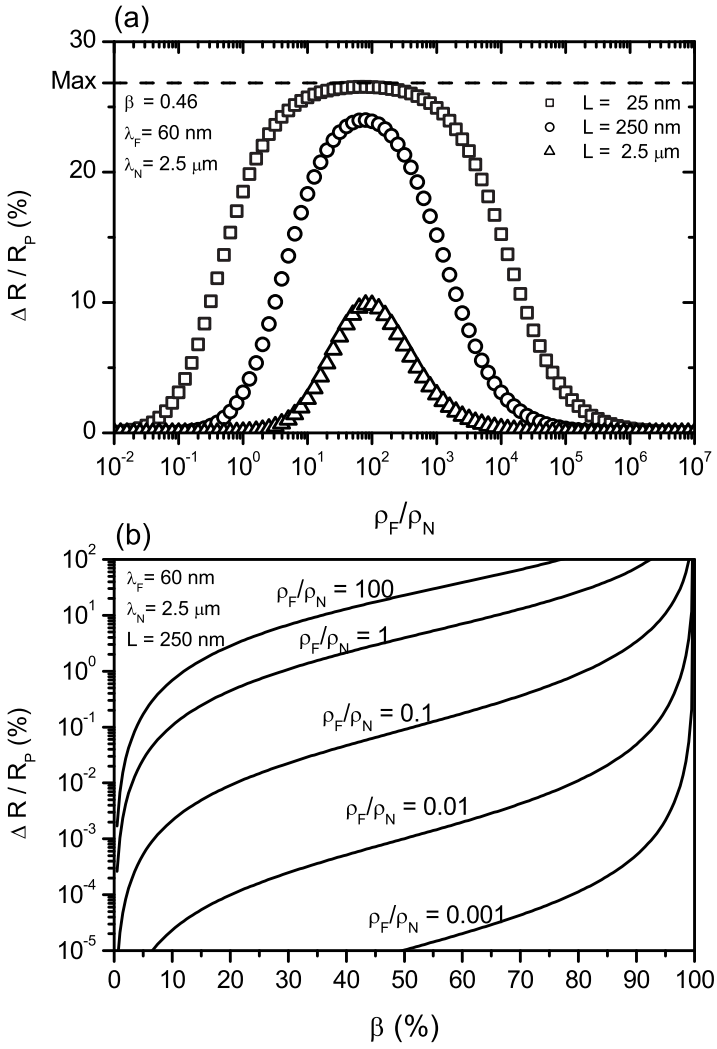


Figure 2.5: (a) The variation of $\Delta R/R_P$ as a function of $\rho_F/\rho_N$ according to Eq. 2.26. Tuning of $\rho_F$ or $\rho_N$ is necessary in order to maximize the magnetoresistance signal. (b) $\Delta R/R_P$ as a function of $\beta$ for several values of $\rho_F/\rho_N$.

increasing the resistivity of the non-magnetic material. In view of this simple model which neglects the ferromagnet metal/semiconductor properties and the transport mechanism in the semiconductor, using Co and pentacene to build spin valves is problematic, since their conductivities are many orders of magnitude different.

## 2.2 Photoelectron spectroscopy (PES) principles

In this section we review some aspects of the photoelectron spectroscopy (PES) technique which are relevant in understanding the results presented in this thesis. The discussion is focused on measurement of solid surfaces. First, we introduce the photoelectric effect and its (electrical) measurement scheme. Subsequently, we discuss two main applications of PES: (a) the determination of the work function (for a metallic surface) and (b) the determination of the (interfacial) energy level alignment at a metal-semiconductor interface. For more details on PES we refer the reader to e.g. [15, 17–20].

### 2.2.1 The photoelectric effect

In a PES experiment, electrons from the occupied energy levels of the sample are excited by irradiation (photoelectric effect). This results in a distribution of photoelectrons which can escape to vacuum, provided that the photoelectrons have sufficient kinetic energy ($E_K$), larger than the work function of a metallic sample or the ionization energy for a semiconducting sample. The photoelectrons are then collected and analyzed as a function of their kinetic energy by an electron analyzer (spectrometer). The measured photoelectron distribution (spectrum) consists of a series of peaks which map the (occupied) energy levels of the sample. The process is schematically shown in Fig. 2.6 for a metallic sample. The kinetic energy of the photoelectron is essentially the difference between the energy of the system with N electrons and the energy of the system with N-1 electrons plus a free electron. Therefore, final state screening effects (relaxation processes that occur faster than the photoemission process) contribute to the kinetic energy of the photoelectron. The photoelectric equation expresses the energy conservation of the process

$$E_B^V = h\nu - E_K - E_{relax} \tag{2.27}$$

where $E_B^V$ represents the binding energy of a certain level with respect to the vacuum level, $h\nu$ is the radiation energy, $E_K$ is the kinetic energy of the photoelectron and $E_{relax}$ is the energy gain by relaxation processes. Note that $E_B^V$ depends on the work function of the sample. High energy photons are used for probing core levels whereas low energy photons are used for probing the valence band. Generally, the photoelectric process can be described as a three step process [18]: the photoexcitation, the transport to the surface and the penetration through the surface of the photoelectrons, see Fig. 2.7b).

1. In the *photoexcitation step*, at any given depth in the sample, light creates electrons which map the density of states of the sample. The photoelectrons that reach the detector without energy loss (elastic collisions only)

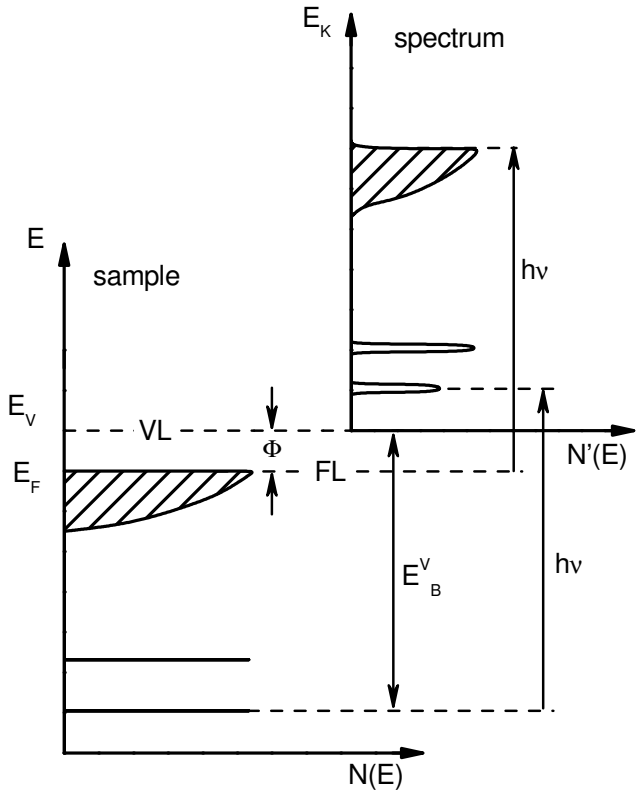


Figure 2.6: Schematic of the photoelectric effect of a metallic sample. The sample is represented by the valence band (dashed area) and some core levels. FL, VL and Φ represent the Fermi level, vacuum level and the work function of the sample. The kinetic energy scale of the excited photoelectrons has its origin at the vacuum level.

are known as primary photoelectrons (peaks). Since the electrons of different atomic systems have different binding energies, the primary peaks are unique to an atomic species and are used to identify the composition of the sample. Therefore, it is possible to identify whether oxidized atomic species exists along with unoxidized ones. The measured number of photoelectrons originating in a certain energy level is proportional to: (a) the cross section of interaction of the light with the wave function associated with the electron, (b) the total number of electrons residing in the respective energy level and (c) the transmission of the detector at the respective kinetic energy. Therefore, the relative intensity of two peaks characteristic

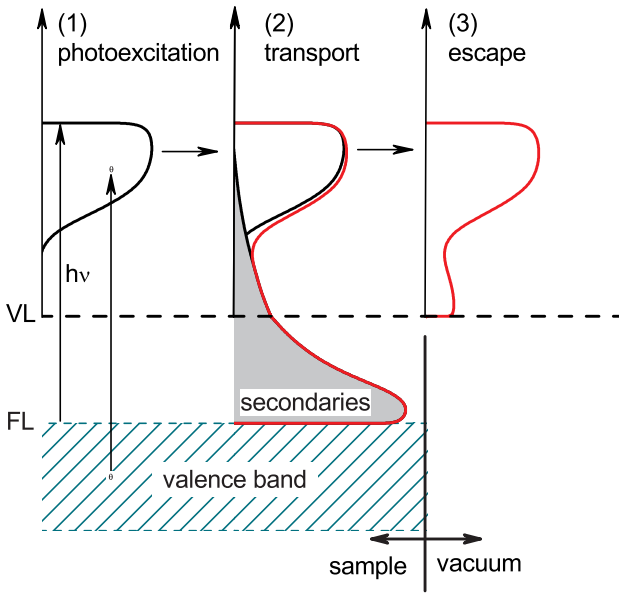


Figure 2.7: Photoelectric effect as a three step process.

of two different atomic species does not equal the relative proportions of the respective atomic species in the sample. However, given an experimental setup, a fixed proportionality factor exists which can be used to perform a quantitative analysis.

Additional peaks arise in the spectrum due to Auger processes [19], interaction with plasmons, band gap excitations etc. These effects are not discussed here.

2. In the *transport step* the photoelectron distribution created at any given depth in the sample travels towards the surface of the sample and may undergo elastic (see previous) or inelastic scattering processes with the atomic systems present in the sample. Besides inelastic interactions in which the photoelectrons loose a discrete amount of energy (such as the interaction with plasmons) a significant part of them will undergo random inelastic collisions loosing partially (or totally) their kinetic energy. These are known as secondary electrons (secondaries) and do not carry information on the initial kinetic energy they acquired. The secondaries cause a raising background on the low kinetic energy side of each primary peak and determine the spectrum to have a finite intensity up to zero kinetic energies.

3. The third step is the *escape step*. All the photoelectrons reaching the sample

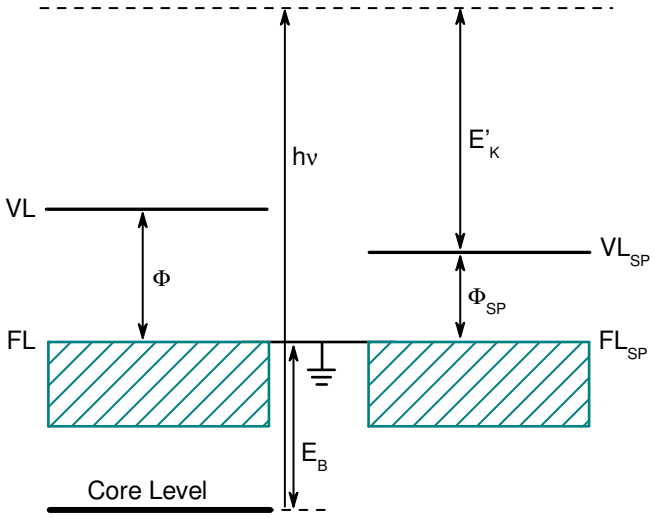


Figure 2.8: Measurement scheme of the photoelectric effect on a metallic sample. The Fermi level of the sample (FL) is brought in electrical equilibrium with that of the spectrometer ($FL_{SP}$) by grounding. $\Phi$ ($\Phi_{SP}$) and VL ($VL_{SP}$) represent the work function and the vacuum level of the sample (spectrometer). An electron with a binding energy $E_B$ is detected having a kinetic energy $E'_K$.

surface can escape to vacuum (and be measured by the spectrometer) only if they have a kinetic energy larger than the surface potential, i.e., larger than the work function for a metallic sample. The work function practically cuts the spectrum, a fact which allows its determination by PES (discussed later).

### 2.2.2 PES measurement scheme

Fig. 2.8 shows the photoelectric effect measurement scheme of a metallic sample in electrical equilibrium with the spectrometer (both are grounded) [20]. For solid samples the origin of the binding energy scale is taken at the Fermi level and not at the vacuum level. According to Fig. 2.8, the photoelectric equation (neglecting the relaxation term) becomes

$$E_B = h\nu - E'_K - \Phi_{SP} \tag{2.28}$$

where $\Phi_{SP}$ represents the work function of the spectrometer and $E'_K$ the measured kinetic energy by the spectrometer. In this way the binding energies become a standard (do not depend intimately on the work function of the sample). It is

clear from Fig. 2.8 that the electrons are accelerated (decelerated) when traveling towards the detector if the spectrometer work function is lower (higher) than the work function of the sample. In the case of deceleration some of the photoelectrons will not arrive at the detector due to the $\Phi_{SP} - \Phi$ field, causing the zero kinetic energy cut-off to deviate from the true cut-off of the spectrum. In order to avoid this situation often a negative bias is applied to the sample. Eq. 2.28 becomes

$$E_B = h\nu - E'_K - \Phi_{SP} - V_{ext} \tag{2.29}$$

where $V_{ext}$ is negative if negative bias (with respect to the grounded spectrometer) is applied.

### 2.2.3 Work function determination by PES

The PES measurement is widely used to extract the work function (ionization potential) of a metallic (semiconducting) sample [20]. Two cut-offs exist in the spectrum: the Fermi cut-off and the secondary electrons cut-off. The Fermi cut-off is determined by electrons originated at the Fermi level which escaped the sample with no loss of energy and are the most energetic photoelectrons that are measured ($E_K'^{max}$). Some of the Fermi level electrons become secondary electrons which determines the spectrum to have finite intensity at all kinetic energies down to zero, even though the density of states corresponding to their kinetic energy is zero. Since only the photoelectrons with a kinetic energy above the work function can escape to vacuum, the work function determines the low kinetic energy cut-off of the spectrum ($E_K'^{min}$). It is now easy to realize (graphically by using Fig 2.7) that the width of the spectrum is exactly the difference between the light energy and the work function of the sample. Therefore, the work function can be calculated according to

$$\Phi = h\nu - (E_K'^{max} - E_K'^{min}) \tag{2.30}$$

With the same formula, the ionization potential of molecules or semiconducting samples can be calculated. A small correction should be applied to Eq. 2.30 which is due to spectrometer broadening.

### 2.2.4 Energy level alignment by PES

The small escape depth of the photoelectrons (tens of Å, depending on their kinetic energy) [18] makes PES a very surface sensitive technique since only a few monolayers beneath the surface of the sample are measured. This allows the investigation of interface formation of semiconductors on metals. In figure 2.9, we present a schematic drawing of a PES measurement of the interface formation

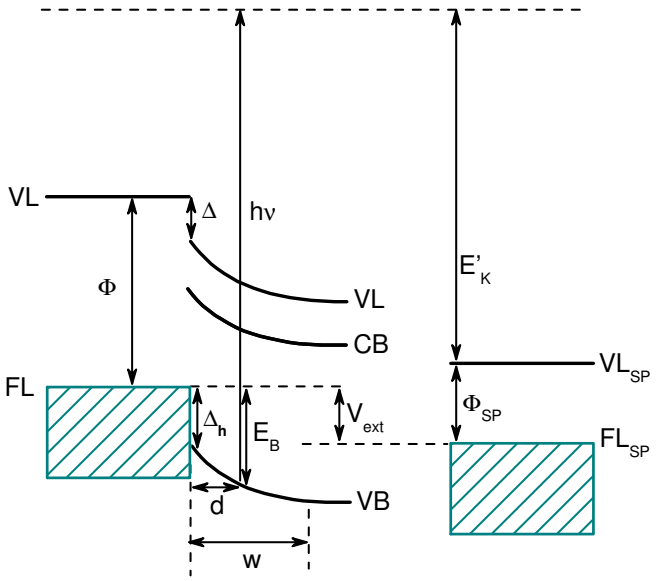


Figure 2.9: Schematic of the interface formation between a metal and an organic semiconductor and the PES measurement. VL, FL, $\Phi$ and $\mathrm{VL}_{SP}$, $\mathrm{FL}_{SP}$, $\Phi_{SP}$ represent the vacuum level, the Fermi level and the work function of the sample and spectrometer, respectively. $w$, $\Delta$ and $\Delta_h$ represent the depletion width, the interfacial dipole and the hole injection barrier, respectively.

between a metal and a semiconductor. The energy level alignment scheme includes an interfacial dipole (vacuum level misalignment). The sample is negatively biased ($V_{ext}$) with respect to the spectrometer detector for reasons described above. Important to note is that the binding energies of the core level electrons depend on their position with respect to FL. By neglecting the metal layer screening (image potential contribution), polarization effects (the screening determined by neighboring semiconductor atoms or molecules) and assuming that there is no chemical interaction between the semiconductor and the metal, the binding energy of the electronic levels is determined by the band bending alone.

Due to the limited escape depth of the photoelectrons, by depositing the semiconductor in steps on top the metal and performing the PES measurement after each deposition step one can probe experimentally the band bending in the semiconductor as a function of its thickness $d$.

To summarize, we exemplify how the interfacial energy level alignment (interfacial dipole and the hole injection barrier) can be determined experimentally from PES measurements. A complete discussion of the interface formation be-

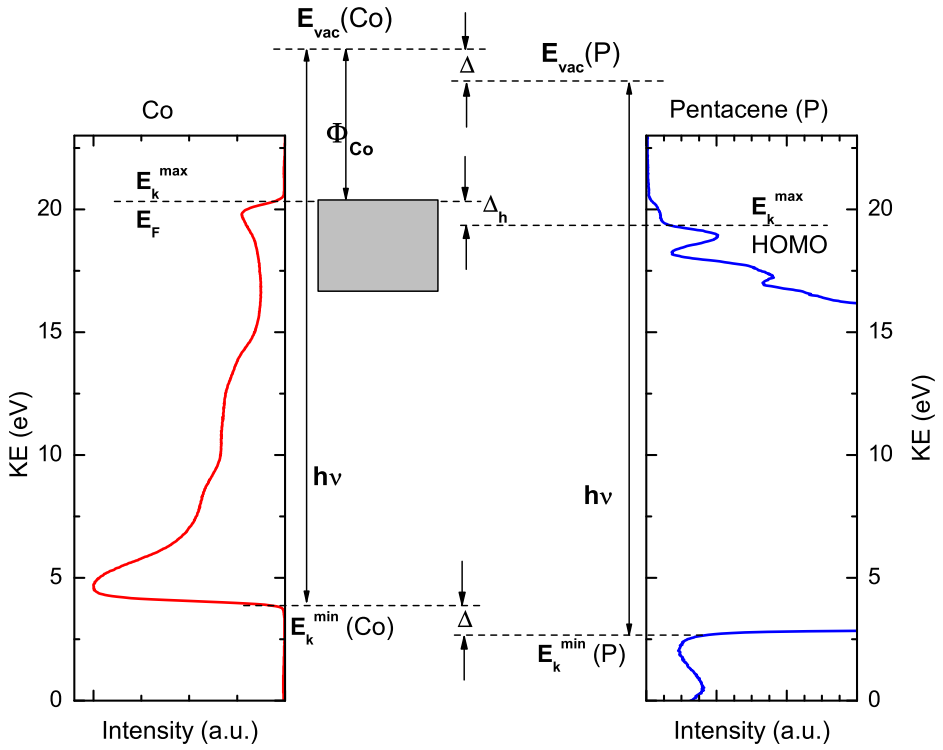


Figure 2.10: Schematic of the interface formation between Co and pentacene as deduced from PES measurements (see text). Left: the spectrum of a thin film of Co. Right: the spectrum of 30 Å pentacene deposited on Co. For clarity purposes the pentacene spectrum is cut and the spectrometer broadening has been neglected.

tween pentacene and Co is presented in *Chapter 4*. Fig. 2.10 shows on the left side the measured spectrum of Co. The measurements were performed using UV light of 21.2 eV, $\Phi_{SP} = 5.0$ eV and $V_{ext} = -4.0$ V bias applied to the sample. The electrons with the highest kinetic energy ($E_K^{max}$) are detected around 20 eV, in agreement with Eq. 2.29 where $E_B = 0$ eV was taken for the FL level electrons. The FL level cut-off position is invariant, being determined by the external bias and the spectrometer work function. In contrast, the secondary electron cut-off (SEC), at the low kinetic energy side ($E_K^{min}$) of the spectrum, is depending on the work function of the sample. The vacuum level position can now be determined graphically by taking the origin at the SEC and measuring a distance equal to the light energy $h\nu$. Upon depositing 30 Å pentacene, the SEC position has changed due to the change in vacuum level position. The interfacial dipole represents the

difference between the vacuum level of Co and that of pentacene, and is given by the shift of the secondary electrons cut-off. Low intensity from the FL electrons of Co can also be seen in the figure. The distance between the leading edge of the highest occupied molecular orbital of pentacene (HOMO level) and the Fermi level represents the hole injection barrier $\Delta_h$. By performing the PES measurement as a function of pentacene thickness, a band diagram can be constructed.

## 2.3 Concluding remarks

In this chapter we briefly reviewed some important aspects of spin transport and photoelectron spectroscopy. In order to efficiently inject and detect spins in semiconductors, conductivity matching of the injector/detector and semiconductor is necessary.

The work function of Co is about 5.0 eV whereas the ionization potential of pentacene is about 4.9 eV. A simple application of the Mott-Schottky rule of vacuum level alignment would predict a nearly ohmic contact which, in view of the conductivity mismatch problem, would not allow for efficient spin injection and detection. However, if a Schottky barrier forms at the interface, then under certain bias conditions efficient injection can be realized. It is therefore of interest to study the interfacial energy level alignment (interfacial dipole, hole injection barrier, band bending, chemical interaction) of pentacene with Co (and in the case of inserting tunnel barriers as well) by photoelectron spectroscopy experiments.

Even though our discussion was not exhaustive, we hope that we provided the reader with the basics to understand the results presented in this thesis.

# References


[1] P. C. van Son, H. van Kempen, and P. Wyder, Phys. Rev. Lett. **58**, 2271 (1987)

[2] G. Schmidt, D. Ferrand, L. W. Molenkamp, A. T. Filip, and B. J. van Wees, Phys. Rev. B, **62**, R4790 (2000)

[3] G. Schmidt, and L. W. Molenkamp, Semicond. Sci. Technol., **17**, 310 (2002)

[4] A. Fert, and H. Jaffres, Phys. Rev. B, **64**, 184420 (2001)

[5] E. I. Rashba, Phys. Rev. B, **62**, R16267 (2000)

[6] S. Datta, *Electronic transport in mesoscopic systems* (Cambridge University Press, Cambridge, England 1995)

[7] E. P. Wohlfarth, *Ferromagnetic materials* (North Holland, 1982), chap. 9, review article *Transport properties of ferromagnets*, I. A. Campbell, A. Fert, p. 747

[8] C. Kittel, *Introduction to solid state physics*, 7th ed. (John Wiley & Sons, Inc., New York, 1996)

[9] T. Valet, and A. Fert, Phys. Rev. B, **48**, 7099 (1993)

[10] F. J. Jedema, H. B. Heersche, A. T. Filip, J. J. A. Baselmans, and B. J. van Wees, Nature **416** 713 (2002)

[11] F. J. Jedema, A. T. Filip, and B. J. van Wees, Nature **410** 345 (2001)

[12] F. J. Jedema, M. S. Nijboer, A. T. Filip, and B. J. van Wees, Phys. Rev. B **67** 85319 (2003)

[13] F. J. Jedema, Ph.D. thesis, University of Groningen, The Netherlands (2002), http://irs.ub.rug.nl/ppn/244584443

[14] A. T. Filip, Ph.D. thesis, University of Groningen, The Netherlands (2002), http://irs.ub.rug.nl/ppn/235146137

[15] H. Ishi, K. Sugiyama, E. Ito, and K. Seki, Adv. Mater., **11**, 605 (1999)

[16] A. Kahn, N. Koch, and W. Gao, J. Polym. Sci., Part B: Polym. Phys., **41**, 2529 (2003)

[17] D. Cahen, and A. Kahn, Adv. Mater., **15**, 271 (2003)

[18] S. Hüfner, *Photoelectron spectroscopy* (Springer-Verlag, 1995)

[19] H. Lüth, *Solid Surfaces, Interfaces and Thin Films* (Springer, 2001), 4th ed.

[20] *Electron Spectroscopy: Theory, Techniques and Applications* vol.2, edited by C. R. Brundle and A. D. Baker, (Academic Press, 1978)